

# Increased Occurrence of Stratospheric Sudden Warmings during El Niño as Simulated by WACCM

MASAKAZU TAGUCHI\* AND DENNIS L. HARTMANN

*Department of Atmospheric Sciences, University of Washington, Seattle, Washington*

(Manuscript received 10 February 2005, in final form 30 June 2005)

## ABSTRACT

Experiments with Whole Atmosphere Community Climate Model (WACCM) under perpetual January conditions indicate that stratospheric sudden warmings (SSWs) are twice as likely to occur in El Niño winters than in La Niña winters, in basic agreement with the limited observational dataset. Tropical SST anomalies that mimic El Niño and La Niña lead to changes in the shape of probability distribution functions (PDFs) of stratospheric day-to-day variability, resulting in a warmer pole and weaker vortex on average for El Niño conditions. The tropical SST forcing induces a response similar to the observed response in the enhancement of the planetary wave of zonal wavenumber 1 (wave 1) and the weakening of wave 2 in the upper troposphere and stratosphere of high latitudes. The enhanced wave 1 contributes to a shift of the PDFs of poleward eddy heat flux in the lower stratosphere, or wave forcing entering the stratosphere. The shift of the PDFs includes an increase of strong wave events that induce more frequent SSWs.

## 1. Introduction

The large interannual variability observed in the Northern winter extratropical stratosphere and troposphere arises from external forcings that vary from year to year, as well as from internal processes that generate unforced variability (Yoden et al. 2002). The external forcings to the extratropical stratosphere and troposphere include the solar cycle, volcanic eruptions, quasi-biennial oscillation (QBO), El Niño–Southern Oscillation (ENSO), and anthropogenic effects (Labitzke and van Loon 1999). This study focuses on the impact of the ENSO on the northern extratropical stratosphere and troposphere.

It has been observed that the northern stratospheric polar vortex tends to be weaker for El Niño winters than for La Niña winters on monthly and seasonal means (van Loon and Labitzke 1987; Labitzke and van Loon 1989). Baldwin and O’Sullivan (1995) also exam-

ined stratospheric variability in relation to tropospheric teleconnections associated with ENSO. van Loon and Labitzke (1987) and Labitzke and van Loon (1999) further mentioned that El Niño winters most often result in (major) midwinter SSWs. In spite of these extensive studies, the observational results are not conclusive by themselves, because it is difficult to demonstrate statistically significant effects of a specific external forcing using the limited observational data. In particular, Hamilton (1993) noted the difficulty of obtaining statistically significant results with the observational record and the problem of separating the effect of ENSO from that of the QBO, because El Niño winters tend to coincide with the easterly phase of the QBO, and vice versa (van Loon and Labitzke 1987; Wallace and Chang 1982). A couple of idealized simulations with general circulation models (GCMs) that include ENSO SST forcings support the earlier observational result of the weaker vortex for El Niño conditions (Hamilton 1995; Sassi et al. 2004).

While most of the observational and modeling studies focused on monthly and seasonal means, the ENSO-induced change in the stratospheric circulation may not be merely a change in the mean states, but it may be important to examine a change in frequency of SSWs (change in shape of PDFs) that characterizes stratospheric variability during winter. This study shows ENSO-induced change in the frequency of SSWs and

---

\* Current affiliation: Department of Earth Sciences, Aichi University of Education, Kariya, Aichi, Japan.

---

*Corresponding author address:* Masakazu Taguchi, Dept. of Earth Sciences, Aichi University of Education, Kariya, 448-8542, Japan.  
E-mail: mtaguchi@aeu.ac.jp

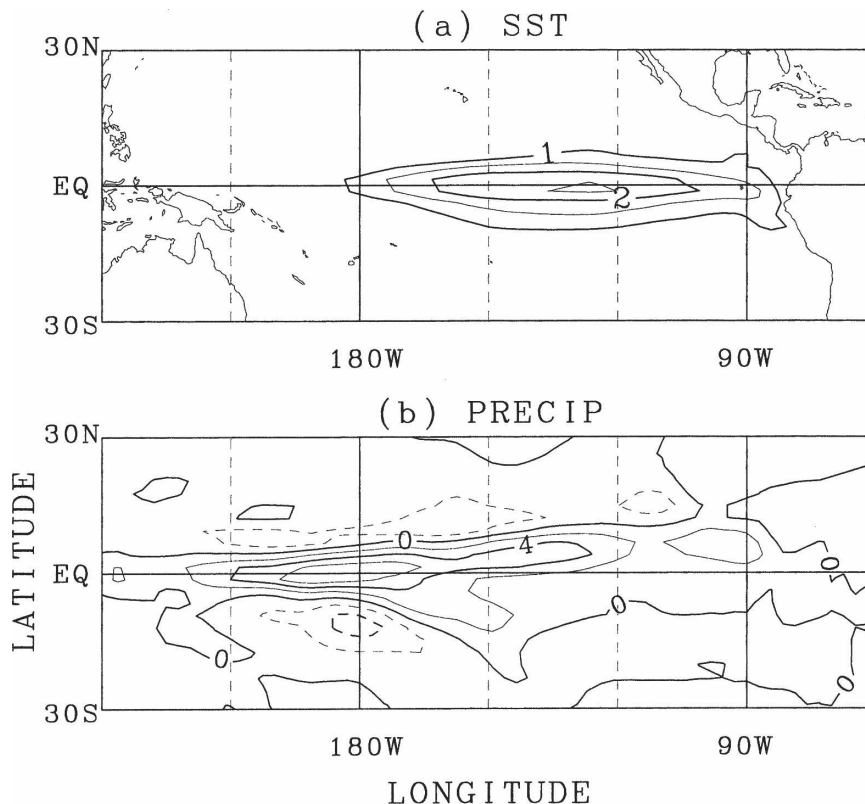


FIG. 1. (a) Imposed SST difference (K), runs WARM - COLD. Contours are drawn from 1 K at a 0.5-K interval. (b) Climatological difference in precipitation rate. Contour interval is 2 mm day<sup>-1</sup>. The longitudinal range is from 120°E to 60°W.

explores the mechanism through dynamical diagnostics by using idealized GCM experiments similar to those of Hamilton (1995) and Sassi et al. (2004). The response of the frequency of SSWs to external forcings remains relatively unexplored. The perspective gained by probing the response of SSWs to external forcing from ENSO will be useful for understanding dynamical processes that govern the troposphere-stratosphere climate system and its response to external forcing.

## 2. Model and experiments

The model used in this study is the Whole Atmosphere Community Climate Model (WACCM), a version of the National Center for Atmospheric Research (NCAR) Community Climate Model that is extended to include the middle and upper atmosphere up to about 110 km altitude (Sassi et al. 2002). The horizontal resolution is T63, with 66 vertical levels. Our experiments consist of two perpetual simulations forced with climatological January conditions including sea surface temperature and zonally symmetric ozone distributions as well as radiative conditions. The ozone distribution is

based on Wang et al. (1995). The two runs are different only in SSTs in the tropical Pacific. The SSTs are lowered for a La Niña-like condition in one run called COLD, while raised for an El Niño-like condition in the other called WARM. The SST difference peaks in the eastern equatorial Pacific at about 2.5 K (Fig. 1a). The model runs are each 9125 days long in this study, which correspond to more than 100 90-day winters. The experiments thus afford a large enough sample to examine change in the frequency of the episodic stratospheric warming phenomenon. Perpetual January experiments are a reasonable first step to study the impact of external forcings on SSW frequency, since interannual variability is largest in midwinter, reflecting the occurrence of SSWs (Labitzke 1982). The imposed SST forcing induces a change in precipitation and atmospheric heating (Fig. 1b). The precipitation response is in good agreement with observations (e.g., Philander 1990).

Taguchi and Hartmann (2005, hereafter TH05) used the same experiments for a shorter period to examine ENSO-extratropical atmosphere connection from a quite different perspective. TH05 showed that warm

ENSO and SSW signals in the extratropical surface climate, though distinct in their hemispheric structures, nonetheless interfere positively over the southeastern United States and northern Mexico to enhance colder and wetter winter climate anomalies there. These anomalies were compared with observed ones and suggest that the WACCM model produces reasonable extratropical tropospheric responses to both ENSO and SSWs. In this paper it is shown that the extratropical response to El Niño-like conditions results in enhanced zonal wavenumber-1 amplitude in high latitudes, forcing more planetary wave energy into the polar stratosphere and hence driving more frequent SSWs.

### 3. Results

The climate of the extratropical stratosphere is warmer for the run WARM than for the run COLD, and the polar night jet is weaker (Figs. 2a,b). The changes in the zonal mean state are driven by enhanced upward propagation of wave activity in the high latitude stratosphere poleward of about 60°N, as measured by the Eliassen–Palm (EP) flux (Fig. 2c). The EP flux used here is the quasigeostrophic scaling (Andrews et al. 1987), which is useful in diagnosing planetary wave activity that can propagate to the stratosphere. The increasing EP flux in the stratosphere can be traced down to the troposphere in lower latitudes around 45°N. These features are very consistent with the results of Sassi et al. (2004), who examined the response of the stratosphere to ENSO in simulations where the SST was specified from observations over the period from 1950–2000.

The daily time series of the zonal mean temperature [T] in the polar middle stratosphere (88°N and 11 hPa, denoted by X in Fig. 2a) is used as an indicator of dynamical conditions in the extratropical stratosphere. Square brackets denote the zonal mean. The polar stratospheric temperature is used because it shows a large climatological difference (Fig. 2a) and day-to-day variation in both runs (not shown). It is very clear that SSWs, or extreme stratospheric anomalies, characterized by large spikes of the temperature time series, are more frequent for the run WARM (Fig. 3). This difference in behavior is robust throughout the runs.

SSWs are defined using the criterion introduced in TH05 for the WACCM runs, and their frequency of occurrence in the two runs is compared. When the polar temperature becomes warmer than 235 K, an SSW is identified and the key day of each SSW is defined to be the day on which the temperature achieved its maximum value. This criterion aims to identify extreme stratospheric events, not distinguishing between major

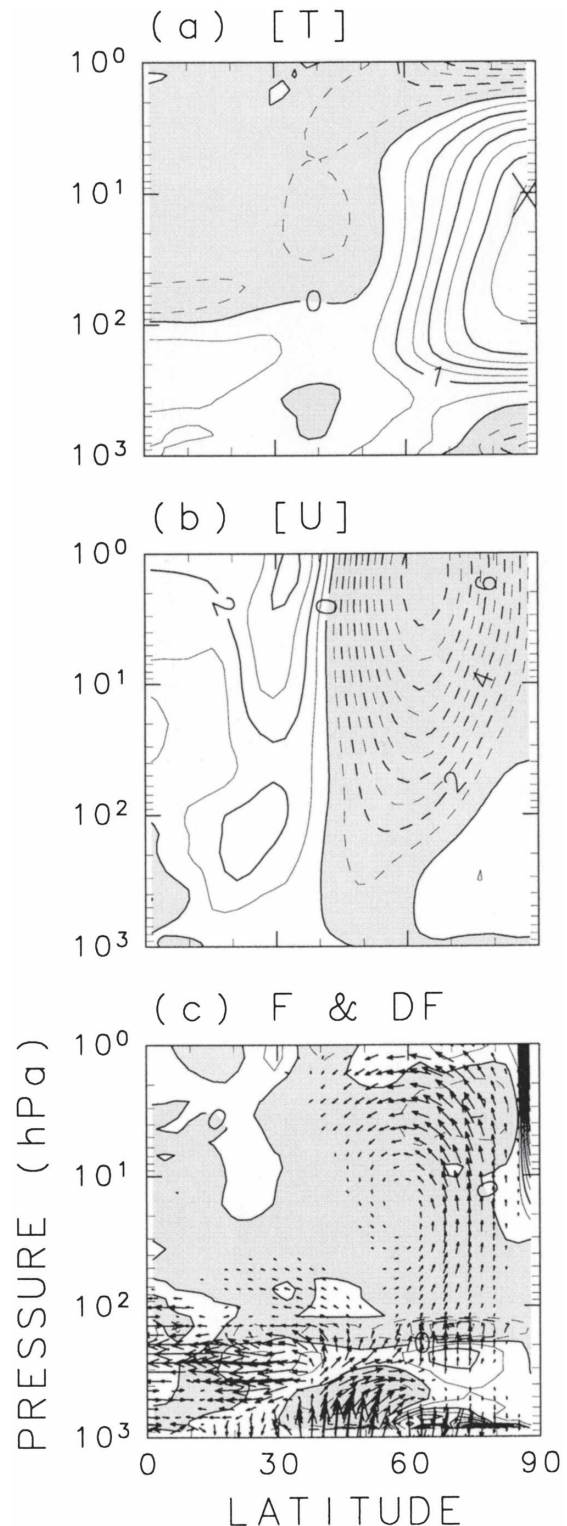


FIG. 2. Climatological difference, runs WARM – COLD: (a) zonal mean temperature [T] (K), (b) zonal mean zonal wind [U] ( $\text{m s}^{-1}$ ), and (c) EP flux F (arrows) and its divergence DF (contours and shades;  $\text{m s}^{-1} \text{ day}^{-1}$ ). The EP flux is divided by the square root of  $1000/\text{pressure}$ .

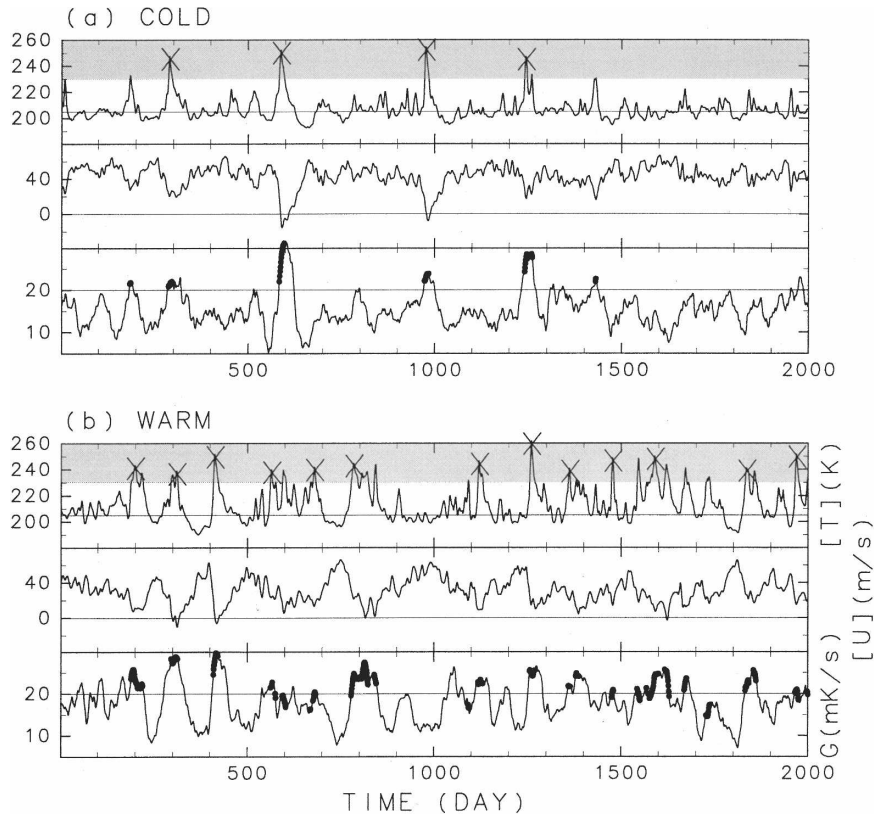


FIG. 3. Daily time series for the first 2000 days in (a) run COLD and (b) run WARM, including the zonal mean temperature  $[T]$  at  $88^{\circ}\text{N}$  and 11 hPa in the top of each panel, the zonal mean zonal wind at  $60^{\circ}\text{N}$  and 11 hPa in the middle, and poleward eddy heat flux averaged at  $45^{\circ}\text{--}75^{\circ}\text{N}$  at 101 hPa at the bottom. The heat flux plotted on each day is averaged for 40 days prior to the day (denoted by G). (top) For  $[T]$ , the crosses denote key days of SSWs (see text for details). The shading denotes a range higher than 230 K. Thresholds of (middle)  $0\text{ m s}^{-1}$  and (bottom)  $20\text{ mK s}^{-1}$ . Filled circles in bottom indicate days when the temperature is in the shaded range.

and minor warmings. This method is based on the previous studies (Yoden et al. 1999; Taguchi 2003). Based on this definition, SSWs are twice as likely to occur for the run WARM (52 events identified in the 9125-day period) as for the run COLD (26 events). The defined key days are denoted by the crosses in Fig. 3 for a 2000-day period.

The difference of the frequency of the SSWs is highly statistically significant according to a Monte Carlo simulation. The test shows that such a bias in events (52 versus 26) occurs by chance in only 22 of 10 000 trials if the probability of an event is equal for the two runs. The change in the frequency of SSWs (or highly disturbed periods) is robust as clearly seen in the temperature time series (Fig. 3). The temperature is a good index for SSWs and closely related to possible alternative indices, such as the zonal mean zonal wind at  $60^{\circ}\text{N}$  and 11 hPa (also plotted in Fig. 3). The variability of the wind corresponds well (though not perfectly) to that of

the temperature with correlation coefficients of  $-0.75$  and  $-0.78$  in the runs COLD and WARM for the 9125 days, respectively, so that the difference in the frequency of SSWs is also clear in the zonal wind time series. It is worthwhile to note that 6 out of the 26 SSWs in the run COLD are major SSWs where the zonal wind is negative, while the run WARM has 12 major warmings out of the 52 SSWs.

The occurrence of SSWs can be related to poleward eddy heat flux in the lower stratosphere of high latitudes ( $45^{\circ}\text{--}75^{\circ}\text{N}$ ), as shown for example by Polvani and Waugh (2004) and Yoden et al. (1999) among others. The heat flux is proportional to the vertical component of the quasigeostrophic EP flux. Polvani and Waugh (2004) also showed that stratospheric anomalies are best correlated with the lower stratospheric heat flux when it is averaged (or cumulated) for the prior 40 days or longer. Figure 3 also shows for each day the heat flux averaged for the prior 40 days (denoted by G). As ex-

pected, in both runs temperatures higher than 235 K are well related with strong heat fluxes more than about  $20 \text{ mK s}^{-1}$ . The correlation coefficients are 0.66 and 0.69 in the runs COLD and WARM, respectively, for the whole simulation period. Such strong wave-driving events are more frequent for the El Niño run WARM.

To relate heat flux and polar temperature anomalies more clearly, two-dimensional PDFs are plotted in Fig. 4 for the two runs, as well as one-dimensional PDFs for each quantity. The change in the frequency of SSWs is reflected in different shapes of 1D PDFs for the temperature. Extreme high values of polar temperature are much more common for the run WARM (El Niño), while the mode temperatures are similar for the two runs (around 200 K). The shapes of the 2D PDFs confirm that the samples of high temperatures correspond well to those of strong eddy heat flux for both runs as examined in Fig. 3. The El Niño-like SST forcing shifts the PDF of the heat flux and polar temperature toward higher values, which is consistent with the increase in frequency of strong wave events and hence SSWs.

Figure 5a plots the difference of the 9125-day mean poleward eddy heat flux in the lower stratosphere (101 hPa) between the two runs as a function of zonal wavenumber and latitude. The mean heat flux is the time average of daily heat flux and includes contributions of both stationary and transient waves. The difference shows that the shift of the 1D PDFs of the heat flux of all waves (Fig. 4) is attributable to planetary wave of

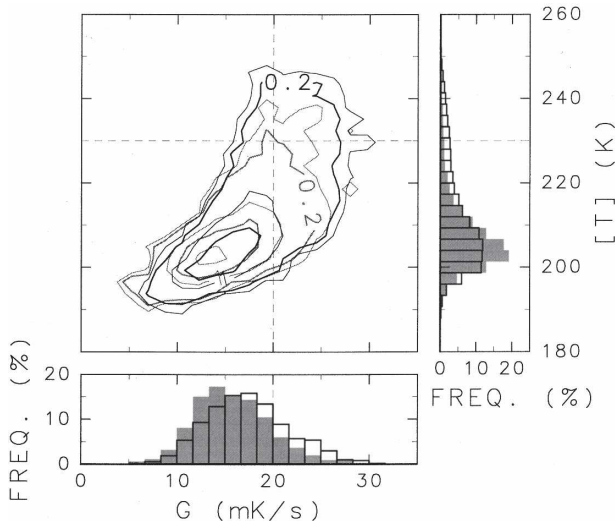


FIG. 4. Two-dimensional PDFs (%) with respect to the polar stratospheric temperature and lower stratospheric time-averaged heat flux for the whole 9125 days. The quantities are calculated as in Fig. 3. Contours are drawn for 0.1%, 0.2%, 1%, 2%, and 4%. One-dimensional PDFs are also drawn for each quantity. Black contours and lines are used for the run WARM in both 2D and 1D PDFs. Broken lines denote 230 K and  $20 \text{ mK s}^{-1}$ .

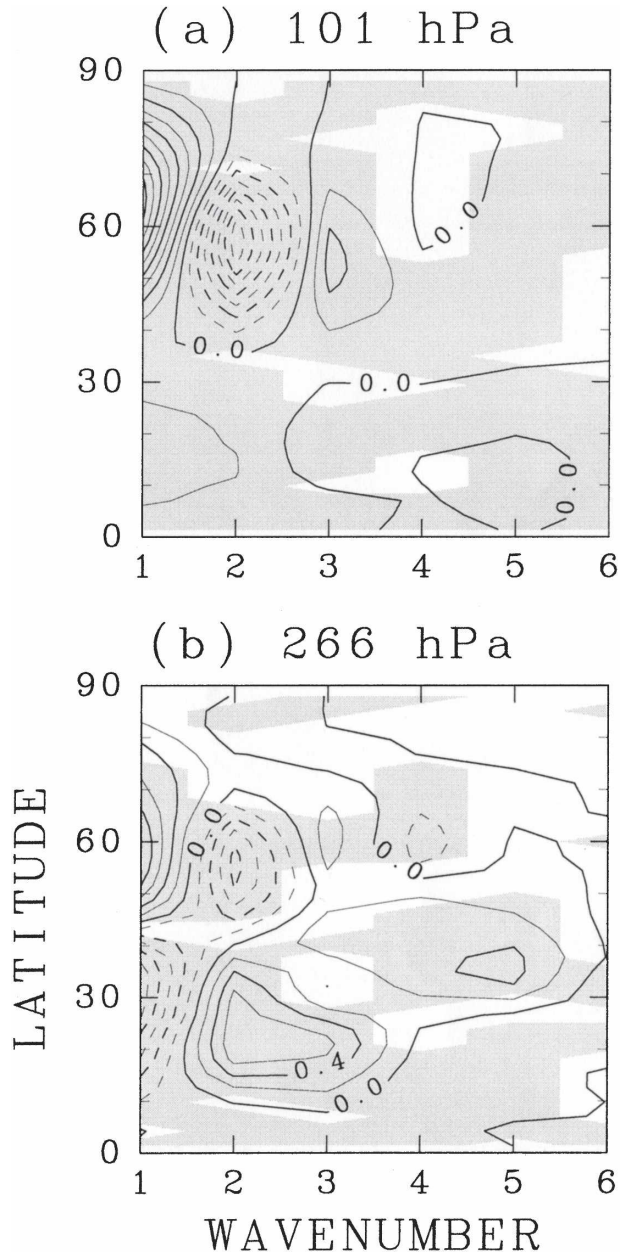


FIG. 5. Difference, runs WARM – COLD, of 9125-day mean poleward eddy heat flux as functions of zonal wavenumber and latitude at (a) 101 and (b) 266 hPa. Contour interval is (a) 0.5 and (b)  $0.2 \text{ mK s}^{-1}$ . Shading indicates that the difference is statistically significant at a 95% confidence level.

zonal wavenumber 1 (wave 1) around  $60^\circ\text{N}$ . The increase of the time-mean heat flux of wave 1 in high latitudes reflects a shift of its daily heat flux (as seen in Fig. 4 for all waves) in the run WARM (not shown). The increase of wave-1 heat flux is also noticeable in the upper troposphere at 266 hPa (Fig. 5b). The difference of the time mean heat flux at the two levels is

basically statistically significant at a confidence level of 95% (denoted by shading in Fig. 5) according to a Student's  $t$  test. In the test, we took account of actual temporal degree of freedom for the heat flux at each wavenumber and latitude (Bretherton et al. 1999). The difference of wave-1 amplitude of geopotential height has similar patterns to Fig. 5 at both levels (not shown). The increased wave-1 activity in high latitudes is important for the increase in frequency of SSWs, since wave 1 can propagate to the stratosphere most easily (Charney and Drazin 1961) and be directed toward the polar region as inferred from Fig. 2c. The amplitude and heat flux of wave 2 decrease for the run WARM, so that the relative importance of wave 1 to wave 2 increases for the El Niño-like condition. This wavenumber shift is consistent with observational work of Quadrelli and Wallace (2002), who noted that the structure of the annular mode of variability has more wave-2 features during La Niña years and more wave-1 features during El Niño years. This change in mode structure is reproduced by the current simulations (not shown).

To understand how the SST forcing induces the wave-1 amplification, Fig. 6 plots stationary wave patterns of geopotential height in the upper troposphere (300 hPa) for the two runs, together with a difference field. Since extratropical low-frequency variations, including the Pacific–North America (PNA) pattern, are equivalent barotropic as is well known (Horel and Wallace 1981; Hoskins and Karoly 1981), the upper tropospheric level is chosen as a representative level to characterize the tropospheric response. The difference pattern in Fig. 6c bears a strong similarity to the height pattern that is correlated with the cold tongue index of ENSO (e.g., Quadrelli 2004) suggesting again that WACCM simulates a realistic response to ENSO variations. Our difference plot also looks similar to the existing GCM experiments (Hamilton 1995; Sassi et al. 2004). A Student's  $t$  test is applied to the height difference at each longitude–latitude gridpoint as in Fig. 5. It shows that the difference is statistically significant at a 95% level for most regions as denoted by shading in Fig. 6d.

Figure 7 shows the longitudinal structure of the geopotential height waves averaged from 50° and 70°N where the heat flux of wave 1 shows the largest response (Fig. 5). The wave field includes a wave-1 component, with ridge and trough around 30°W and 150°E (60°W and 120°E) near 60°N for the run WARM (COLD), respectively (Figs. 6 and 7). The wave-1 amplitude is about twice as large in the run WARM than in the run COLD.

The change in relative importance of wave 1 to wave 2 (Fig. 5) implies a change in dominant synoptic pat-

terns of SSWs between the two runs. To examine this possibility, we obtain amplitude of waves 1 and 2 at 60°N and 11 hPa for a mature stage (between two days before and after the key days) for all SSWs (Fig. 8). Consistent with the increase of wave-1 activity (Fig. 5), the plot shows that the El Niño-like SST forcing results in increase of wave-1-type SSWs (polar vortex shift) and decrease of wave-2-type SSWs (vortex split) for the run WARM. In other words, the run WARM favors wave-1 SSWs, while wave-2 events occur more frequently for the run COLD. These features in the stratospheric synoptic patterns are consistent with the results of van Loon and Labitzke (1987), Hamilton (1995), and Sassi et al. (2004).

The demonstration of greater frequency of SSWs for El Niño conditions is obtained for an idealized perennial January situation, which gives the advantage that statistically significant results can be obtained with minimal computational expense. The present results can be compared with a more realistic 50-yr WACCM simulation forced with observed SSTs from 1950 to 1999 (Sassi et al. 2004), and with National Center for Environmental Prediction (NCEP)–NCAR reanalysis data from 1979–99 (Kalnay et al. 1996). All three datasets show a similar tendency for more samples of high temperatures during El Niño years (Fig. 9).

For the Sassi et al. dataset, La Niña and El Niño conditions are defined here as December–February (DJF) winters when DJF-mean SSTs averaged over 180°–90°W and 6°N–6°S are in the bottom and top 15 of 50 values, respectively (see the figure caption for the explicit classification of the two groups). Each group therefore includes  $15 \times 90 = 1350$  days. A similar tendency for warmer polar temperatures is also found for NCEP–NCAR reanalysis data from 1979 to 1999 (Fig. 9c). Only the postsatellite period is used to ensure the homogeneity of the data. In this case, the La Niña and El Niño groups are each defined with the same SST index to include six subsets (540 days) of the whole 21 DJF samples. Referring to the SSWs defined in TH05 for the real world, the La Niña group of the six DJF samples has three SSWs while six SSWs occur in the six El Niño DJF samples. Although the Sassi et al. (2004) and NCEP–NCAR data show similar signals to the present work, it is difficult to demonstrate statistical significance in the change in frequency of SSWs for both the 50-yr WACCM run and observations because the samples are not large enough. The details of the changes in the PDFs are different between the datasets because of their differences in sample size and nature. As mentioned in the introduction, another problem in attributing the observed difference in the PDFs to the ENSO is the phase overlap between the ENSO and

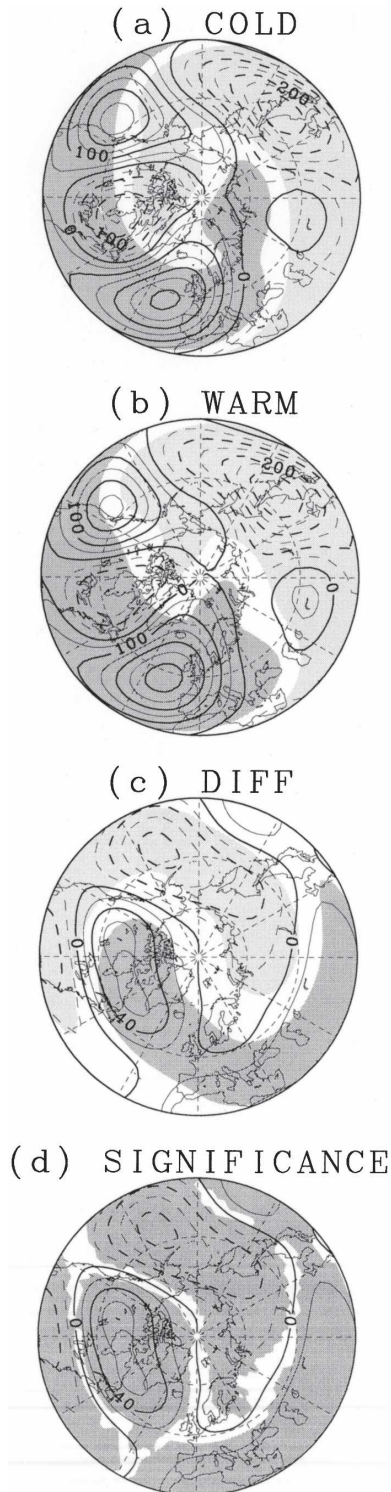


FIG. 6. Stationary wave patterns (m) of geopotential height at 300 hPa for runs (a) COLD, (b) WARM, and (c) WARM - COLD. Contours are for all waves. Dark and light shadings denote values larger than 25 m and smaller than -25 m for a wave-1 component, respectively. (d) The difference, again, for all waves in contours. The shading indicates that the difference is statistically significant at a 95% confidence level. Outermost circle is 30°N, and broken lines denote latitudes of 50° and 70°N.

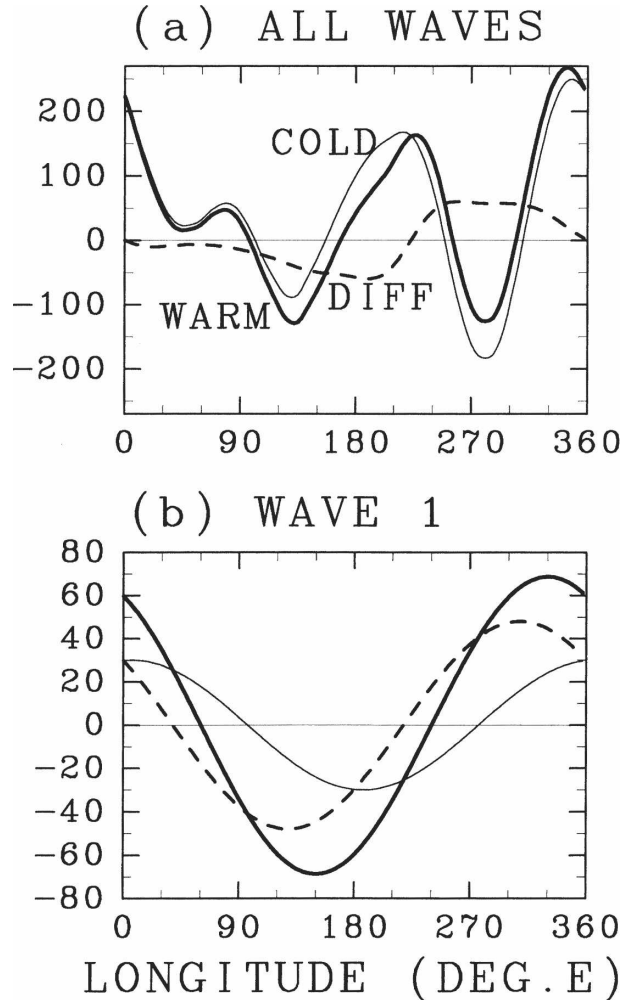


FIG. 7. Geopotential height waves (m) averaged between 50° and 70°N at 300 hPa as functions of longitude for (a) all waves and (b) wave 1. Thin and thick solid lines are for runs COLD and WARM, respectively. Broken line is for difference, runs WARM - COLD.

QBO (Hamilton 1993), although the phase overlap itself remains an open question in its details and mechanism. In the present calculations, however, the QBO effect is not present and the perennial January simulation allows a sufficient sample to be obtained that the differences are statistically significant, and can be uniquely related to the imposed ENSO-like SST forcing.

#### 4. Summary

The intermittent occurrence of SSWs is a vital aspect of the troposphere-stratosphere climate system especially in the Northern Hemisphere during winter. Our analysis of the WACCM experiments under perpetual

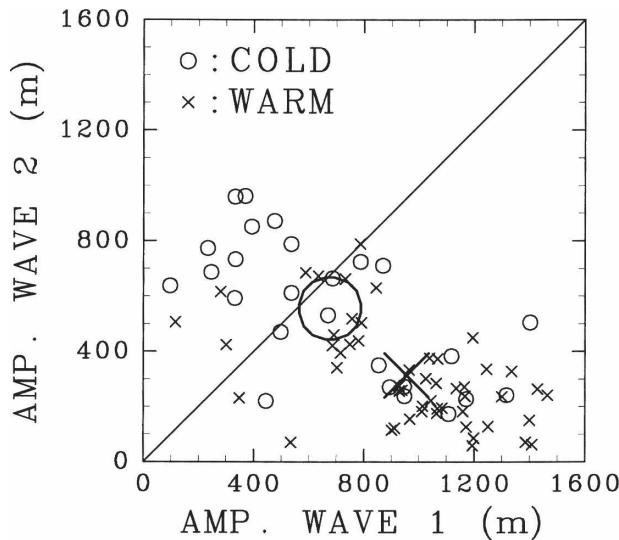


FIG. 8. Scatterplot between amplitude of waves 1 and 2 of geopotential height at 60°N and 11 hPa for a mature stage of 26 and 52 SSWs in the runs COLD (dots) and WARM (crosses), respectively. Average is denoted by the big symbol for each run.

January conditions gives a clear indication that the frequency of SSWs increases during El Niño. The El Niño-like SST condition induces an increase in planetary wave-1 amplitude in the high latitude troposphere and an increase in the planetary wave-1 driving of the stratosphere by the troposphere in high latitudes, compared to the La Niña-like SST condition. El Niño also seems to shift the wave driving from wave 2 to wave 1, which leads to more efficient wave propagation. The

changes in the PDFs for the planetary heat flux and for the polar stratospheric temperature are different. The increase of the wave-1 heat flux or wave forcing appears primarily as a shift of the PDFs to higher values.

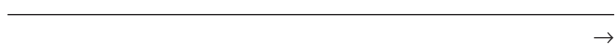
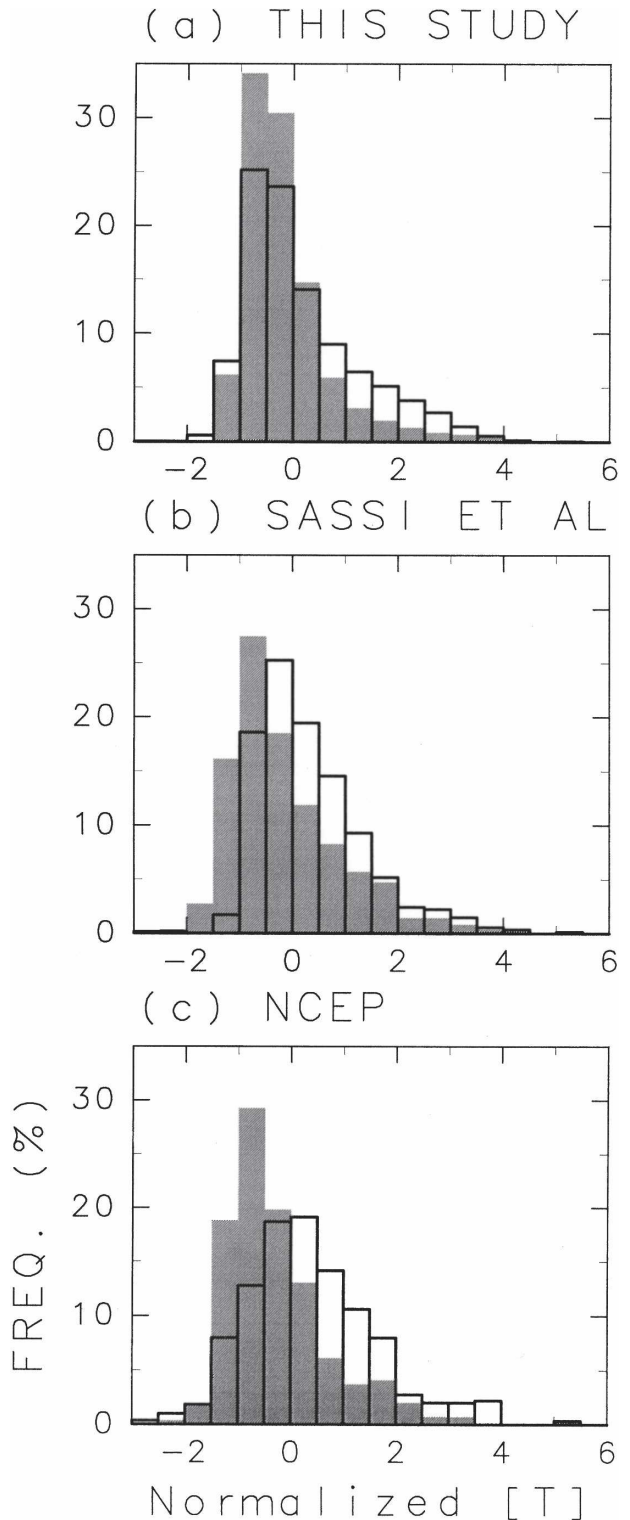


FIG. 9. (a) PDFs (%) of the zonal mean temperature at 88°N and 11 hPa for the runs COLD (shading) and WARM (solid line). The temperature values are normalized with the mean and standard deviation of all data combined for the two runs. (b) As in (a), but for the zonal mean temperature at the same grid point in a 50-yr WACCM simulation forced with observed SSTs from 1950 to 1999 (Sassi et al. 2004). Shading and solid line are for 15 La Niña and El Niño DJF winters, respectively, which are determined with DJF mean SSTs averaged over 6°N–6°S, 180°–90°W. The La Niña years are 1950, 1951, 1955, 1956, 1963, 1965, 1968, 1971, 1974, 1975, 1976, 1985, 1989, 1996, and 1999. The El Niño years are 1952, 1958, 1964, 1966, 1969, 1970, 1973, 1977, 1980, 1983, 1987, 1988, 1992, 1995, and 1998. These years denote the years to which January belongs. The temperatures on each calendar day are normalized with the mean and standard deviation for the day calculated from the 50-yr data. (c) As in (b), but for the temperature at the North Pole (NP) and 10 hPa in the NCEP–NCAR reanalysis data from 1979 to 1999. The La Niña and El Niño winters include six DJF winters (1984, 1985, 1989, 1996, 1997, 1999 vs 1983, 1987, 1988, 1992, 1995, 1998) when the SSTs in the region are in the bottom and top 6 of 21 values, respectively.



The PDF of polar stratospheric temperature is suggested to not merely shift, but to change shape giving a similar mode value, but a much greater probability of extreme warm events for El Niño conditions than for La Niña conditions.

The present results suggest very strongly that ENSO has a strong and systematic effect on the stratosphere. The model results are consistent in form and substance with observational evidence, but are much more convincing because of the ability of the modeling approach to both isolate the effect of ENSO from other influences and also conduct a long enough integration to obtain statistically significant results. Additional work on the effect of ENSO on the detection of trends in stratospheric climate and the possible interaction between changes in tropical and stratospheric climate should be encouraged by these results. Initial results on the interaction of ENSO with stratospheric climate change will be reported elsewhere.

*Acknowledgments.* We thank the developers at NCAR for the use of WACCM. We also thank Marc L. Michelsen for assisting our model runs. The present graphic tools were based on the codes in the GFDL-DENNOU Library. This work is supported by the NSF under Climate Dynamics Grants ATM-0332269 and ATM-9873691 to the University of Washington.

#### REFERENCES

- Andrews, D. G., J. R. Holton, and C. B. Leovy, 1987: *Middle Atmosphere Dynamics*. Academic Press, 489 pp.
- Baldwin, M. P., and D. O'Sullivan, 1995: Stratospheric effects of ENSO-related tropospheric circulation anomalies. *J. Climate*, **8**, 649–667.
- Bretherton, C. S., M. Widmann, V. P. Dymnikov, J. M. Wallace, and I. Blade, 1999: The effective number of spatial degrees of freedom of a time-varying field. *J. Climate*, **12**, 1990–2009.
- Charney, J. G., and P. G. Drazin, 1961: Propagation of planetary-scale disturbances from the lower to the upper atmosphere. *J. Geophys. Res.*, **66**, 83–109.
- Hamilton, K., 1993: An examination of observed Southern Oscillation effects in the Northern Hemisphere stratosphere. *J. Atmos. Sci.*, **50**, 3468–3473.
- , 1995: Interannual variability in the Northern Hemisphere winter middle atmosphere in control and perturbed experiments with the GFDL SKYHI general circulation model. *J. Atmos. Sci.*, **52**, 44–66.
- Horel, J. D., and J. M. Wallace, 1981: Planetary-scale atmospheric phenomena associated with the Southern Oscillation. *Mon. Wea. Rev.*, **109**, 813–829.
- Hoskins, B. J., and D. J. Karoly, 1981: The steady linear response of a spherical atmosphere to thermal and orographic forcing. *J. Atmos. Sci.*, **38**, 1179–1196.
- Kalnay, E., and Coauthors, 1996: The NCEP/NCAR 40-Year Reanalysis Project. *Bull. Amer. Meteor. Soc.*, **77**, 437–472.
- Labitzke, K., 1982: On the interannual variability of the middle stratosphere during the northern winters. *J. Meteor. Soc. Japan*, **60**, 124–139.
- , and H. van Loon, 1989: The Southern Oscillation. Part IX: The influence of volcanic eruptions on the Southern Oscillation in the stratosphere. *J. Climate*, **2**, 1223–1226.
- , and —, 1999: *The Stratosphere*. Springer, 179 pp.
- Philander, S. G. H., 1990: *El Niño, La Niña, and the Southern Oscillation*. Academic Press, 289 pp.
- Polvani, L. M., and D. W. Waugh, 2004: Upward wave activity flux as precursor to extreme stratospheric events and subsequent anomalous weather regimes. *J. Climate*, **17**, 3548–3554.
- Quadrelli, R., 2004: Patterns of wintertime climate variability of the Northern Hemisphere wintertime circulation. Ph.D. thesis, University of Washington, 188 pp. [Available online at <http://www.atmos.washington.edu/%7eroberta/>]
- , and J. M. Wallace, 2002: Dependence of the structure of the Northern Hemisphere annular mode on the polarity of ENSO. *Geophys. Res. Lett.*, **29**, 2132, doi:10.1029/2002GL015807.
- Sassi, F., R. R. Garcia, B. A. Boville, and H. Liu, 2002: On temperature inversions and the mesospheric surf zone. *J. Geophys. Res.*, **107**, 4380, doi:10.1029/2001JD001525.
- , D. Kinnison, B. A. Boville, R. R. Garcia, and R. Roble, 2004: Effect of El Niño–Southern Oscillation on the dynamical, thermal, and chemical structure of the middle atmosphere. *J. Geophys. Res.*, **109**, D17108, doi:10.1029/2003JD004434.
- Taguchi, M., 2003: Tropospheric response to stratospheric sudden warmings in a simple global circulation model. *J. Climate*, **16**, 3039–3049.
- , and D. L. Hartmann, 2005: Interference of extratropical surface climate anomalies induced by ENSO and stratospheric sudden warmings. *Geophys. Res. Lett.*, **32**, L04709, doi:10.1029/2004GL022004.
- van Loon, H., and K. Labitzke, 1987: The Southern Oscillation. Part V: The anomalies in the lower stratosphere of the Northern Hemisphere in winter and a comparison with the quasi-biennial oscillation. *Mon. Wea. Rev.*, **115**, 357–369.
- Wallace, J. M., and F.-C. Chang, 1982: Interannual variability of the wintertime polar vortex in the Northern Hemisphere middle stratosphere. *J. Meteor. Soc. Japan*, **60**, 149–155.
- Wang, W.-C., X.-Z. Liang, M. P. Dudek, D. Pollard, and S. L. Thompson, 1995: Atmospheric ozone as a climate gas. *Atmos. Res.*, **37**, 247–256.
- Yoden, S., T. Yamaga, S. Pawson, and U. Langematz, 1999: A composite analysis of the stratospheric sudden warmings simulated in a perpetual January integration of the Berlin TSM GCM. *J. Meteor. Soc. Japan*, **77**, 431–445.
- , M. Taguchi, and Y. Naito, 2002: Numerical studies on time variations of the troposphere-stratosphere coupled system. *J. Meteor. Soc. Japan*, **80**, 811–830.